EXPERIMENTAL INVESTIGATION OF SECOND SOUND SHOCK WAVES IN LIQUID HELIUM II

Thesis by

Philip Louis Rogers

In Partial Fulfillment of the Requirements

for the Degree of

Aeronautical Engineer

California Institute of Technology

Pasadena, California

1979

(Submitted October 13, 1978)

ACKNOWLEDGEMENTS

It is a great pleasure to thank all of the people who gave their time and effort during the course of this investigation. The support of my advisor, Professor Hans W. Liepmann, is gratefully acknowledged.

I should like to thank my fellow student, Jack Wise, whose able assistance was always available. The cheerful cooperation of Mr. Earl Dahl in the construction of the experimental apparatus and in solving many of the day-to-day problems encountered is greatly appreciated. The help of Dr. Harris A. Notarys of Low Temperature Physics was indispensible for the thin film fabrication.

I should also like to thank Mrs. Betty Wood for her help with the figures and Ms. Marcia Clark for typing the manuscript and for her friendship.

Last, but not least, there is my wife Lisa, without whose unending devotion and love, this project could never have been accomplished.

This project was funded by the Air Force Office of Scientific Research.

To LISA, my little d.f.

ABSTRACT

Second sound shock waves in liquid helium II were studied experimentally using superconducting thin film detectors. The temperature waves were generated electrically using an evaporated thin film heater and the effects of variations in pulse power (input power to the heater as large as 150 Watts/cm^2) and pulse duration (from less than 100 μsec to 10 msec) were examined. A number of different materials were tested for use as detectors with the best results obtained from evaporated gold on tin.

Qualitative agreement with Khalatnikov's theory was obtained; however, breakdown of the theoretical model was observed for heater input powers greater than 20 - 30 Watts/cm^2, in agreement with other known results. Quantitative data for shock strength, i.e., temperature amplitude, wave speed, and pulse power, were obtained. The critical counterflow velocities calculated from these data, $w = 2.51$ to 3.77 m/sec, indicate that heat fluxes at least an order of magnitude greater than those reported for steady channel flow can be transported using the pulsed techniques.

TABLE OF CONTENTS

LIST OF FIGURES

I. INTRODUCTION

A. Background

Liquid helium, when cooled below 2.17° K, experiences a so-called λ-transition from liquid helium I to liquid helium II. Helium I behaves as a classical fluid; however, helium II exhibits non-classical behavior which can only be explained by using the concepts of quantum mechanics.

Below the λ-point, liquid helium behaves as if it were composed of two interpenetrating, noninteracting fluids: superfluid carrying no entropy and having no viscosity and normal fluid having entropy and viscosity. This two-fluid model has been used to explain many of the anomalous properties of liquid helium II.

From this two-fluid model, one can deduce two distinct forms of wave motion. When the two fluids move in phase, an ordinary pressure or sound wave is produced. However, when the two fluids move out of phase, a temperature wave, termed "second sound", is transmitted and is unique to liquid helium II. As with ordinary pressure waves, the temperature waves are non-linear in that their propagation speeds are not, in general, equal to their acoustic speeds. Hence finite amplitude perturbations can steepen to form shock waves.

The importance of these temperature waves can best be realized by a consideration of heat transfer by the liquid helium. Liquid helium II exhibits the ability of transferring large amounts of heat at practically zero temperature gradient. This phenomenon,

which is very much like that of an ordinary heat pipe, is of great importance in the cooling of superconducting magnets and other devices. However, it has been found that for heat fluxes beyond a critical value, this "supra heat conduction" breaks down, for which an adequate explanation and description does not yet exist.

Much work has been done, both experimentally and analytically, in investigating second sound waves. In particular, second sound shock waves were first observed by Osborne (1) in 1950. Later, Dessler and Fairbank (2) in 1956 studied the amplitude dependence of the second sound velocity by using a small amplitude marker pulse, first alone, and then superimposed on a larger amplitude carrier wave and comparing the times of flight.

Several optical investigations have been carried out. In 1967, Coulter, Leonard and Pike (3) used focussed shadowgraph and schlieren techniques to study the heat transport from a wire to helium II and were able, although with very poor resolution, to see second sound waves. More recently, Gulyaev (4, 5) in 1969 and 1970 optically studied large amplitude second sound using a schlieren system and constantan ribbons spaced 1 mm apart.

Cummings (6) in 1975 and later Cummings et al. (7) in 1977 studied both first sound (pressure) and second sound shock waves in helium II by using a specially constructed cryogenic shock tube to generate both pressure and temperature shocks and then later by electrically pulsing a heater and measuring the time of flight of the temperature shock waves produced.

The present investigation is an attempt to extend these results

with special emphasis on studying the critical breakdown of the superfluid heat conduction properties.

B. Theoretical Formulation

To develop the hydrodynamic equations of liquid helium II, we will follow Landau (8, 9) and consider the liquid helium II as composed of two fluids, the superfluid (denoted by subscript s) and the normal fluid (subscript n). We assume that the density of the liquid helium can be written as the sum of the superfluid density and the normal fluid density

$$\rho = \rho_s + \rho_n \ .$$

Also, the momentum density can be written as the sum of the superfluid and normal fluid momentum densities

$$\vec{j} = \rho\vec{v} = \rho_s\vec{v}_s + \rho_n\vec{v}_n \ .$$

Then, neglecting dissipative processes, the two-fluid conservation equations of mass, momentum and entropy can be written in the usual way

$$\text{MASS} \qquad \frac{\partial \rho}{\partial t} + \vec{\nabla} \cdot \vec{j} = 0$$

$$\text{MOMENTUM} \qquad \frac{\partial \vec{j}}{\partial t} + \vec{\nabla} \cdot \vec{\vec{\pi}} = 0$$

$$\text{ENTROPY} \qquad \frac{\partial \rho s}{\partial t} + \vec{\nabla} \cdot (\rho s \vec{v}_n) = 0$$

where $\vec{\vec{\pi}} = \rho_s \vec{v}_s \vec{v}_s + \rho_n \vec{v}_n \vec{v}_n + p\vec{\vec{I}}$

and $\vec{\vec{I}}$ is the identity tensor.

Two more equations are necessary to close the system. Hence, along with an equation of state, we may write an equation of motion for the superfluid alone. Since the superfluid is an ideal, irrotational fluid, we may write

$$\vec{\nabla} \times \vec{v}_s = 0 \ .$$

Consequently, $\vec{v}_s$ is the gradient of a scalar potential, and this potential can be identified as the chemical potential per unit mass, μ. Then the superfluid equation of motion can be written as

SUPERFLUID MOTION

$$\frac{\partial \vec{v}_s}{\partial t} + \vec{\nabla}\left(\tfrac{1}{2} v_s^2 + \mu\right) = 0 \ .$$

The boundary conditions at a solid surface require that the tangential component of $\vec{v}_n$ vanish from the no-slip condition, the normal component of the mass flux $\vec{j}$ vanish since there can be no mass flux through the surface, and the normal component of heat flux $\vec{q} = \rho s T \vec{v}_n$ be continuous. The set of equations, together with the boundary conditions, constitute the two-fluid hydrodynamic model for liquid helium II.

In order to extract the acoustic speeds for first and second sound, we linearize the hydrodynamic equations. With $\vec{w}$ denoting the relative velocity between the normal fluid and superfluid, $\vec{w} = \vec{v}_n - \vec{v}_s$, the linearization is performed by assuming that $\vec{v}$ and $\vec{w}$ are small, and considering small perturbations in ρ, p, T, and s about their equilibrium values. The linearized equations

can then be written

$$\frac{\partial \rho}{\partial t} + \vec{\nabla} \cdot \vec{j} = 0$$

$$\frac{\partial \vec{j}}{\partial t} + \vec{\nabla} p = 0$$

$$\frac{\partial \rho s}{\partial t} + \rho s \vec{\nabla} \cdot \vec{v}_n = 0$$

$$\frac{\partial \vec{v}_s}{\partial t} + \vec{\nabla} \mu = 0 \ .$$

These four equations can be reduced to two wave equations by using thermodynamic identities for μ and p, and

$$\frac{\partial^2 \rho}{\partial t^2} = \nabla^2 p$$

$$\frac{\partial^2 s}{\partial t^2} = \left(\frac{\rho_s}{\rho_n}\right) s^2 \quad \nabla^2 T \ .$$

By assuming fluctuations proportional to $e^{-i\omega(t - x/C)}$ where C is a wave speed, the equations can be reduced to

$$C^4 - C^2 \left[\left(\frac{\partial p}{\partial \rho}\right)_s + \frac{\rho_s}{\rho_n} \frac{T s^2}{C_v} \right] + \frac{\rho_s}{\rho_n} \frac{T s^2}{C_v} \left(\frac{\partial p}{\partial \rho}\right)_T = 0$$

which has solutions, with $\left(\frac{\partial p}{\partial \rho}\right)_s \doteq \left(\frac{\partial p}{\partial \rho}\right)_T$ from $Cp \doteq C_v$ for liquid helium II,

$$C_{10}^2 = \left(\frac{\partial p}{\partial \rho}\right)$$

$$C_{20}^2 = \frac{\rho_s}{\rho_n}\frac{Ts^2}{C_p}$$

The first is the familiar sound speed while the second is the second sound acoustic speed. For first sound, the density or pressure fluctuations can be seen to be first order and $\vec{v}_s \doteq \vec{v}_n \doteq \vec{v}$: the entire liquid moves as a whole; while for second sound the entropy or temperature fluctuations are first order and $\vec{j}$ and $\vec{v}$ are approximately zero : the two fluids (normal and super) move in opposite directions.

Khalatnikov (10) determined the governing equations and jump conditions for both first and second sound shock waves by expanding the thermodynamic variables ρ, s, and μ in terms of p, T, and the relative velocity w, and retaining terms of order w^2. For temperature discontinuities, Khalatnikov found that the second sound shock speed C_2 can be expressed as

$$C_2 = C_{20}\left[1 + \frac{\Delta T}{2}\frac{\partial}{\partial T}\ell n\left(C_{20}^3\frac{\partial s}{\partial T}\right)\right]$$

and

$$w = \left(\frac{\rho}{\rho_n}\frac{s}{C_{20}}\right)\Delta T \quad .$$

Recall that C_{20} is the second sound acoustic speed and was found to be

$$C_{20} = \left(\frac{\rho_s}{\rho_n} \frac{T s^2}{C_p} \right)^{\frac{1}{2}} .$$

The non-linearity of the second-sound wave can easily be seen from the expression for C_2 since the wave speed depends on the temperature jump ΔT. Note that the coefficient of the ΔT term changes its sign for $1.87^{\circ} K < T < 2.17^{\circ} K$ and hence it is possible for a negative ΔT to propagate as a shock wave in this temperature range.

The heat flux in the second sound wave, as stated above, can be expressed as

$$\dot{Q} = \rho s T v_n .$$

From the definition of the relative velocity $\vec{w} = \vec{v}_n - \vec{v}_s$ and $\vec{j} = \rho \vec{v} = \rho_s \vec{v}_s + \rho_n \vec{v}_n = 0$ for pure counterflow (as is the case for second-sound waves; i.e., no net mass flow), the heat flux can be written in terms of w:

$$\dot{Q} = \rho_s s T w .$$

Hence a critical heat flux implies a critical relative velocity and vice versa.

In an attempt to explain the sudden appearance of this critical heat flux, Gorter and Mellink (11) postulated a mutual friction mechanism between the super and normal fluids with a friction force proportional to w^3 and appended such a term to the hydrodynamic equations. Many measurements have been made of this critical

counterflow, all done in narrow channels with steady flow. In an attempt to correlate these previous measurements, Dimotakis (12) derived a relatively simple similarity law from a dimensional consideration of the hydrodynamic equations with the mutual friction terms added. For steady flow in channels, this law implies a critical value for the counterflow velocity w_c and hence for the critical heat flux $\dot{Q}_c$ as

$$w_c d \doteq \frac{1}{\pi \rho_s A}$$

where d is the diameter of the tube and A is the coefficient in the Gorter-Mellink term, given by the empirical formula (13)

$$\log_{10} A(T) = 1.10 + 3.12 \log_{10} T + \frac{0.0076}{1 - T/T_\lambda} .$$

The aims of this investigation, then, are to quantify, with experimental data, the non-linearity of the second sound shock speed and to study the critical heat flux phenomenon discussed above. Second sound shock waves are ideal for this purpose as the shock speed (and hence amplitude) is dependent on the heat input. Consequently, for a known heat input pulse, a measurable and repeatable wave is produced. Since all previous measurements of critical counterflow have been done with steady flow, an investigation can be made into the effects of nonsteady heat transfer (using these temperature shock waves) on the critical counterflow velocity. These results can then be used to determine the validity of the Dimotakis

similarity law in nonsteady flow.

II. EXPERIMENTAL APPARATUS

A. Shock Tube

The method chosen as the most practical for producing the second sound shock waves consisted of electrically pulsing a suitable heating element and following the wave thus produced as it travels along a tube. Since, from the two-fluid model, heat is convected away by the normal fluid, and the total mass flux in the tube is zero, a counterflow is set up when the heating element is pulsed, creating a temperature wave.

The "second sound shock tube" designed and constructed for this investigation consists of a one inch square cross section Plexiglas tube with provisions for a heater at one end and temperature detectors at the opposite end and also along one sidewall. The shock tube is shown in Figure 1. The heater mounts on the flange at the bottom and sealing is attempted using a silicon rubber "gasket". Detectors, which will be discussed below, can be mounted on the top of the four inch long tube, for endwall measurements, and also along the removable sidewall by spring clamping a glass sensor slide in place. Since all structural parts are constructed from Plexiglas, there can be no differential shrinkage and hence all angular alignments are maintained when the shock tube is cooled to liquid helium temperatures. The entire shock tube assembly is immersed in liquid helium and since it is not completely sealed, the liquid helium can fill the tube. All work is done at the saturated vapor pressure with the height of liquid above

the tube providing enough hydrostatic pressure above SVP to allow the firing of at least smaller heat pulses without significant boiling.

B. Heater

Several considerations affected the design of the heating element used to produce the second sound shock waves. First, the element should be capable of withstanding large voltage pulses, on the order of 100 - 200 volts. Second, the heater must have a very fast time response in order to closely follow the shape of the voltage input. Finally, the heater assembly must be able to survive repeated cycling to liquid helium temperatures.

In order to get the necessary time response, it was decided to use a thin film element as the heater. After much experimentation with different substances, it was found that Nichrome, vacuum evaporated onto a quartz substrate to a thickness of approximately 1000 angstroms, gave the best results in terms of film electrical resistance (the order of 10 ohms) and durability. Quartz was chosen as a substrate for its good thermal properties, especially its strength when cooled to liquid helium temperatures.

Electrical contact to the heater film was accomplished by evaporating 1000 Å thick copper pads at the edges of the Nichrome film and attaching the input wire leads by mechanical clamps, using coiled indium wire between the clamp and the evaporated copper pad. This method of attaching the leads proved very satisfactory and gave no major problems. Sufficient force could be applied to compress the indium wire to insure electrical contact

when cooled to liquid helium temperatures. A photograph of a typical heater appears in Figure 2.

The electrical heater pulse is created by a specially designed pulser, capable of generating pulses of up to 100 volts amplitude and duration ranging from several microseconds to over 10 milliseconds. Furthermore, the high voltage pulser can follow any input waveform, in order to see the effects of a slowly rising heat pulse on the shock wave produced. An oscilloscope trace of a typical voltage pulse is shown in Figure 3.

C. Detectors

In order to measure the temperature amplitudes of the second sound shock waves, it was decided to follow an earlier development by Laguna (14) and use superconducting thin films with adjustable transition temperatures. Different superconducting materials and techniques were tried with varied success, including tantalum on titanium, aluminum oxide, and tin on gold, all deposited on various substrates. The tantalum on titanium deposited on silicon proved to be the most durable, and after repeated cycling in liquid helium, showed no sign of degradation. However, the final detectors used , which gave the best results, were gold evaporated on tin, deposited on a quartz or pyrex glass substrate. The reasons for choosing the tin-gold film will be discussed below. Pure tin is vacuum evaporated to form a film 1000 Å thick. Then 250 Å of gold is deposited on the tin and the combination is then photo-etched following a technique used by Laguna (14) to form the actual detector. The detector

consists of a strip of this gold-tin combination, 0.025 mm wide and 10 mm long, with pure tin superconducting leads to make connections to the lead-in cables. These connections are made with pressed indium. A photograph of a typical detector slide is shown in Figure 4. The basic transition temperature of these superconducting thin films is determined by the ratio of gold to tin (pure tin transitions at 3.74^{o} K); however, the transition temperature can be lowered by applying a magnetic field to the film, and by this means the transition temperature can be set to whatever point is desired. The temperature variations due to the passage of the second sound wave cause changes in the film resistance, and with a constant bias current, changes in the voltage drop across it. By adjusting the magnetic field so as to have the film transition to its superconducting state at the working shock tube temperature, as shown in Figure 5, a large slope, $\frac{dV}{dT}$, of voltage drop versus temperature and therefore a large sensitivity, can be obtained. The detectors are calibrated under static conditions by recording the voltage drop across the film for a fixed magnetic field as the bath temperature is slowly varied.

The signal from the detector is then amplified by an ultra low-noise preamplifier (Princeton Applied Research Model 113), and a voltage-time history of the second sound shock passage is recorded on an oscilloscope.

D. Data Reduction Technique

In order to obtain the second sound shock speed, a digital

interval counter (Hewlett-Packard Model 5326B Counter-Timer DVM) with a resolution of 0.1 μsec., is used to measure the time of flight of the wave, either from the heater to the detector, or between two detectors. For the heater to detector case, the counter is triggered on by the voltage pulse into the heater and off by the sensor output. In the detector to detector case the counter measures the time of flight of the wave between two detectors a known distance apart.

Temperature amplitude information can be obtained from the detector voltage-time history recorded on an oscilloscope. The voltage to temperature conversion is determined from the static calibration curves for each sensor, and knowing the amplifier gain, the temperature jump, ΔT, can be determined by measuring the voltage amplitudes from the oscilloscope traces. In this manner, plots of shock strength $\frac{\Delta T}{T}$, versus shock "Mach number" (wave speed divided by the local second sound acoustic speed) and also heater input power versus Mach number can be obtained.

III. RESULTS

The quality of the signal produced from the superconducting detectors is demonstrated in Figure 6. It shows the response of a tin on gold sidewall detector to a heat pulse propagating through the liquid. The wave is travelling from right to left in the photograph and the second sound shock can clearly be seen to be at the front of the pulse. The heat pulse in Figure 6 was generated from a square voltage pulse, similar to the one shown in Figure 3, however of 100 μsec duration. From the fast risetime of the shock (the risetime measured from the photograph is limited by the amplifier bandwidth, the actual risetime is much less than a microsecond) and the low noise level of the signal, very accurate measurements of the wave speed can be made.

Figure 7 shows a series of heat pulses, all produced by rectangular voltage pulses, and it can readily be seen how the heat pulse shape develops as it propagates along the tube. In exact analogy with corresponding piston produced pressure shock waves in gases, it is evident that the trailing edge of the pulse catches up to the shock front. One interesting feature to note in these oscilloscope traces are the small pulses following behind the heat pulse. These "blips" appear in all traces and can be seen to overtake the heat pulse and eventually ride on top of it. These pulses will be discussed in greater detail later on.

Also in analogy with ordinary pressure sound waves, the second sound shock waves reflect from an endwall with a cor-

responding doubling of the amplitude. Figure 8 shows heat pulses reflecting from a solid endwall. The detectors in these photographs are tin on gold sidewall detectors and the upper trace in each oscillograph is a sidewall detector closest to the heater, while the lower trace is one closest to the endwall. Figure 8a shows the reflection of a 10 msec long heat pulse while Figure 8b shows 100 μsec pulses. As before, wave propagation is to the left and the incident wave (on the left) and the reflected wave (on the right) are both clearly visible. The temperature amplitude doubling is readily seen in Figure 8a.

Also apparent in both photographs are the "blips" mentioned above, and the existence of both positive and negative "blips" is clearly evident.

Figure 9 shows oscilloscope traces of heat pulses of various lengths from 250 μsec to 10 msec. There seems to be no qualitative difference in pulse shape from short pulses to long ones except that the trailing edge never overtakes the shock front in the very long pulses, at least in the length of the shock tube.

A superconducting detector was mounted on the end of a probe installed in the center of the shock tube in order to investigate any difference in waveform that may exist between the center and sidewall of the shock tube. Oscilloscope traces of the detector output are shown in Figure 10. The lower traces are the center probe outputs while the upper traces are the sidewall detector outputs. Figure 10a shows 100 μsec long heat pulses and Figure 10b shows

10 msec pulses. In Figure 10b there appears a significant difference between the center and sidewall traces. While this difference is also seen in Figure 10a, the effect is more easily explainable using the longer pulses shown in Figure 10b. Referring to Figure 10c, we note the wave shape: after passage of the shock front, the pulse stays flat for a time of 0.0205 msec corresponding to a length of 0.42 mm (using the second sound acoustic speed C_{20} = 20.41 m/sec for a bath temperature of 1.65° K) or one-half the width of the center probe end. The temperature amplitude decays to one-half the initial amplitude (height h in the drawing) in 0.089 msec corresponding to a distance of 1.817 mm or one-half the length of the sensor strip. From the data collected in endwall measurements, it was found that an end-mounted detector output is twice the amplitude of the incident wave, as was seen from an examination of the reflected wave traces in Figure 8. However, due to the fact that the detector does not occupy the entire area of the shock tube, diffracted waves will be generated at the edges of the detector as the shock front passes, as shown in Figure 10c. These waves cause the amplitude of the reflected wave measured by the end-mounted probe to decay until the amplitude is that of the incident wave. This is the behavior clearly seen in Figure 10b.

As mentioned earlier, a series of alternating positive and negative pulses appears following every heat pulse. Although no conclusive evidence has as yet been obtained, results thus far lead to several possible explanations as to their origin. Perhaps the most plausible origin of these pulses is possible diffracted

waves generated at the edges of the thin film heater, where the shock tube joins the substrate. Although the wavelength of the "blips" and the spacing between the ones in the series do not exactly match the expected values for diffraction waves, the numbers are close enough so as to not be discounted. Attempts were made to seal the joint between the heater film and shock tube; however, it could not be determined if the joint was properly sealed against a "superleak", and since the pulses still appeared, no conclusive results were obtained. The small pulses are definitely not generated by the heater, as there is no possible way to generate a negative temperature wave (below ambient temperature) using an electrically-excited heater. As can be seen from an examination of the heater voltage pulse, shown in Figure 3, there is no evidence of any extraneous pulses which could be causing these "blips". One other possible explanation is the small pulses are evidence of some sort of motion left behind in the wake of the heat pulse, possibly indicative of vortices generated by the passage of the second sound shock pulse. More work needs to be done in order to be conclusive as to the origin of these pulses.

Figures 11 - 14 show plots of shock strength, $\frac{\Delta T}{T}$, versus the ratio of shock wave speed to second sound speed (called "Mach number" in analogy with ordinary gasdynamic shocks) for various detectors and detector locations. Figures 11 and 12 are for end mounted detectors, Figure 11 showing the results obtained from an endwall mounted tantalum-on-titanium detector and Figure 12 showing an endwall tin-on-gold detector along with the results from

the center-probe, also an end mounted tin-on-gold detector. While the qualitative shape of both plots is essentially the same, the shock amplitudes given by the tin-gold detectors are much higher than those from the tantalum. This discrepancy can be explained by considering the composition and construction of the two types of detectors.

The tantalum-titanium detector is fabricated by depositing tantalum on top of titanium which had been deposited on a silicon substrate. The tantalum is then anodized to a certain depth to produce a superconducting transition temperature in the desired range. This produces an oxide layer on top of the actual superconducting detector strip which acts as a thermal insulator for the detector. Hence the detector cannot measure the full temperature jump produced by the shock. In addition, the silicon substrate is an excellent heat conductor, which enhances this problem. To verify this, a tantalum-titanium detector was fabricated on a glass substrate which resulted in significantly higher amplitudes.

Plotted in Figure 12 are data from several different experimental runs as shown, and for three heat pulse lengths: 100 μsec, 3 msec, and 10 msec. As can be seen from the data, there appears to be no appreciable difference in the behavior of the shock wave for the range of pulse lengths used in the initial linear region of the plot. However, the data seem to indicate that the shorter, 100 μsec, pulses were capable of reaching a higher temperature amplitude than the longer pulses. Although more data

need to be obtained, other experimental runs seem to support this observation.

The development of a critical limit of shock strength in the region $1.04 \leqslant M \leqslant 1.06$ is clearly evident in both figures. This behavior will be discussed in greater detail below.

Figure 13 shows a plot of shock strength versus Mach number for a sidewall-mounted tin on gold detector for two different experimental runs. Again the development of this critical limit in shock strength is evident. Note that the temperature amplitudes shown here are one-half those of the endwall measurements, as is expected. Also shown for comparison is a calculation of the shock strength versus Mach number as given by Khalatnikov (10) and developed above. Recall that

$$C_2 = C_{20}\left[1 + \frac{\Delta T}{2}\frac{\partial}{\partial T} ln\left(C_{20}^3 \frac{\partial s}{\partial T}\right)\right].$$

Now with $\frac{\partial s}{\partial T} = \frac{C_p}{T}$, we can write

$$M = \frac{C_2}{C_{20}} = 1 + \frac{\Delta T}{T}\left[\frac{3}{2}\frac{T}{C_{20}} + \frac{\partial C_{20}}{\partial T} + \frac{T}{2C_p}\frac{\partial C_p}{\partial T} - \frac{1}{2}\right].$$

The derivatives appearing in the brackets can be calculated by using the result from Chapter I for C_{20} and the definition of $\rho_s = \rho - \rho_n$ to give

$$C_{20}^2 = \left(\frac{\rho}{\rho_n} - 1\right) s^2 \frac{T}{C_p}.$$

This gives M in terms of temperature derivatives of $\frac{\rho_n}{\rho}$ and C_p, which have been tabulated by Maynard (15). Evaluating the expression for M at the initial temperature of 1.65° K and the corresponding saturated vapor pressure, we find for M in terms of the shock strength

$$M = 1 + 1.4704 \frac{\Delta T}{T} ,$$

which is shown in Figure 13.

The discrepancy between the calculated values of $\frac{\Delta T}{T}$ and the measured values can again be explained in terms of an insulating oxide layer existing on top of the detector film.

Since the detectors are calibrated under static conditions it is not clear that the calibration is valid for the existing dynamic passage of the heat pulse, since in the static case, the film substrate has time to come to equilibrium with the liquid helium bath, while in the actual shock wave case, this certainly does not occur, and hence the film may not be responding properly to the shock amplitude. This could easily be analyzed using the heat equation; however, reliable data for the thermal conductivity and thermal diffusivity could not be found for these materials at liquid helium temperatures.

Shock wave speed, determined by measuring the time of flight between two sidewall detectors, as opposed to measuring time of flight between the heater and detector as in the previous cases, is plotted with shock strength in Figure 14. These data were obtained using gold on tin detectors in order to attempt to further reduce the oxide layer which forms on the tin due to exposure to the atmosphere.

However, due to the relatively thin (250 Å) layer of gold, and the apparent intermingling of the tin and the gold rather than a gold layer forming on top of the tin, a tin oxide layer is still definitely produced. Also, since the problem of the response of the substrate to the wave passage, as already discussed, still exists, the temperature amplitudes measured still are below the calculated values.

The qualitative appearance of the data, however, is considerably different in Figure 14 than in the previous plots. Whereas in the previous figures, the data fold over, but with an apparent increase in wave speed for the same shock strength, no such behavior is seen in Figure 14. In fact, for increasing heater power input, the shock strength increases to a maximum value, $\frac{\Delta T}{T} = 0.0197$ in Figure 14, then folds back on itself unlike the previous measurements. In order to distinguish the higher heat input data (folded portion past the critical limit) from the lower heat values, a different symbol has been used for these points. Thus, a unique shock strength implies a unique wave speed, as would be expected. One plausible explanation for the difference between the two curves (heater to detector and detector to detector measurements) is liquid helium boiling at the heater surface. For the higher amplitude pulses, the liquid helium definitely vaporizes at the heater surface (verified visually and by an audible "clicking" sound). If the wave speed is determined by measuring time of flight from the heater to detector and there is the formation of a vapor bubble, then the actual time

of flight of the wave may not be properly determined. This situation is eliminated by measuring time of flight between two detectors placed far enough downstream so that the shock wave passes by after the heater boiling has stopped. Further verification of this phenomenon is obtained using pulses of 10 msec duration. The heater boiling (i.e., the voltage pulse to the heater) has not stopped before the shock wave passes the detectors and a folding in the curve, similar to the heater to detector case, is observed.

The apparent critical limit in shock strength seen in the data presented could be attributed to liquid boiling behind the shock wave. Since the experiment is conducted at the saturated vapor pressure with only the head of liquid helium above the shock tube, calculations indicate that certain combinations of large amplitude shock waves with lower levels of liquid helium in the bath could result in boiling behind the wave. This would indicate that in order to increase the heat pulse amplitude, a pressurized system is necessary.

Another explanation for the peak in the shock strength is the reaching of the critical limit in heat flux, or counterflow velocity w, as discussed above. While the magnitude of the critical Mach number does not appear very large, the dependence of the heat flux in the wave on the counterflow velocity produced by the shock is very pronounced, as indicated in Figures 15 and 16, where heat flux is plotted against shock Mach number (and hence the counterflow velocity, w, which depends on M) for the heater to detector measurements (Figure 15) and the detector to detector measure-

ments (Figure 16). The heat fluxes plotted in these figures are calculated in the following manner :

Recall that the heat flux can be expressed as

$$\dot{Q} = \rho_s s T w .$$

From the expression for w :

$$w = \frac{\rho}{\rho_n} \frac{sT}{C_{20}} \frac{\Delta T}{T} ,$$

the heat flux can be written

$$\dot{Q} = \rho C_{20} C_p T \frac{\Delta T}{T} ,$$

or

$$\dot{Q} = \rho C_{20}^3 \left(\frac{\rho_n / \rho}{1 - \rho_n / \rho} \right) \left(\frac{C_p^2}{s^2} \right) \frac{\Delta T}{T} .$$

For $T_o = 1.65^o K$,

$$\dot{Q} = 9.1407 \times 10^6 \frac{\Delta T}{T} \quad \frac{\text{Watts}}{m^2} .$$

Since $\frac{\Delta T}{T}$ is related to the Mach number M, $\dot{Q}$ can be expressed in terms of M if desired.

Since the counterflow velocity, w, is related to the shock strength $\frac{\Delta T}{T}$, we can calculate the value of w for the critical limit of $\frac{\Delta T}{T}$ in the data. From

$$w = \left[\frac{\rho}{\rho_n} \frac{sT}{C_{20}} \right] \frac{\Delta T}{T} ,$$

we compute a $w_{max} = 2.51 \frac{m}{sec}$ for $\frac{\Delta T}{T} = 0.018$ and $T_o = 1.6420^\circ K$. This value of w_{max} is at least one order of magnitude greater than previously found for steady channel flow. If the value of w is computed using the Mach number at the observed critical point, which can be related to $\frac{\Delta T}{T}$ by Khalatnikov's theory, then a value of $w = 3.77$ m/sec is obtained, which is even greater than before. Hence, since the critical heat flux is related to the critical counterflow velocity, it would be expected that heat fluxes at least an order of magnitude greater can be transported using pulsed techniques.

If we assume the Dimotakis similarity is valid for this geometry, then a length scale is needed. At least close to the shock front, the critical value for the counterflow velocity cannot depend on the tube dimensions. Hence, the only apparent length scale entering the problem is the shock thickness. Provided the peak in the shock strength data is the critical condition, we can apply the Dimotakis similarity to calculate the shock thickness. Recall that the similarity parameter is expressed as

$$\rho_s A w_c \ell = \text{const} \doteq 1$$

or

$$w_c \ell = \frac{1}{\rho_s A} ,$$

where A is the Gorter-Mellink constant. Using the value of $w_{max} = w_c = 2.51$ m/sec calculated above, we arrive at a length, or shock

thickness, of $\ell = 5.42\ \mu$. Moreover, using the adjusted value of $w_{max} = 3.77$ m/sec, we compute a thickness of $3.61\ \mu$.

Figure 17 shows a plot of heater power versus shock Mach number for two different pulse lengths obtained from detector to detector measurements. It is apparent that the same peak appears in these data as in the amplitude measurements. Very similar data has been published by Cummings et al. (7) and the agreement is extremely good. They find a folding in the curve at the same heater power (about 20 - 30 Watts/cm^2) as is shown here. Note that the initial part of the curve is linear, in agreement with the theory. Also noteworthy are the apparent oscillations in the data for the 250 μsec pulses after the peak in the curve. This behavior was also seen in the data from the center probe measurements, shown in Figure 18. These oscillations can be correlated to the "blips" mentioned above catching up and overtaking the heat pulse. As the alternating positive and negative pulses overtake the heat pulse and shock front, the data undergo the oscillatory behavior shown. There are not enough data to be conclusive as to whether this effect is caused by the "blips", or both caused by a third phenomenon, or whether the correlation is merely coincidental.

IV. CONCLUSIONS

A facility to study second sound shock waves was designed and constructed. Preliminary measurements using superconducting thin film detectors indicate the existence of a critical breakdown of the "supra heat conductivity" of the liquid helium II at much higher heat fluxes than previously measured in the steady flow condition. The ability to transfer larger amounts of heat using pulsed techniques is of great technological importance. Qualitative confirmation of Khalatnikov's linear theory was accomplished, and agreement with other known results was established. Performing these measurements in a pressurized system will definitely shed more light on the question of critical breakdown, as the boiling problem encountered in this investigation will be eliminated.

REFERENCES

1. Osborne, D.V., Proc. Phys. Soc. (London) A64, 114 (1951).
2. Dessler, A.J. and Fairbank, W.M., Phys. Rev. 104, 6 (1956).
3. Coulter, D.M., Leonard, A.C. and Pike, J.G., Advances in Cryogenic Engineering, Vol. 13, Plenum Press, p. 640 (1968).
4. Gulyaev, A.I., Zh. Eksp. Teor. Fiz. 57, 59 (1969).
5. Gulyaev, A.I., Zh. Eksp. Teor. Fiz. Pis. Red. 11, 332 (1970).
6. Cummings, J.C., J. Fluid Mech. 75, 373 (1976).
7. Cummings, J.C., Schmidt, D.W. and Wagner, W.J., Phys. Fluids 21, (5), 713 (1978).
8. Landau, L., J. Phys. USSR 5, 71 (1941).
9. Landau, L.D. and Lifshitz, E.M., Fluid Mechanics, Pergamon Press (1959).
10. Khalatnikov, I.M., Introduction to the Theory of Superfluidity, translated by Pierre C. Hohenberg, W.A. Benjamin, Inc., New York (1965).
11. Gorter, C.J. and Mellink, J.H., Physica 15, 285 (1949).
12. Dimotakis, P.E., Phys. Rev. A, 10 (5) (1974).
13. Dimotakis, P.E. and Broadwell, J.E., Phys. Fluids 16, 1787, (1973).
14. Laguna, G.A., Ph.D. Thesis, California Institute of Technology (1975).
15. Maynard, J., Phys. Rev. B, 14, (9), (1976).

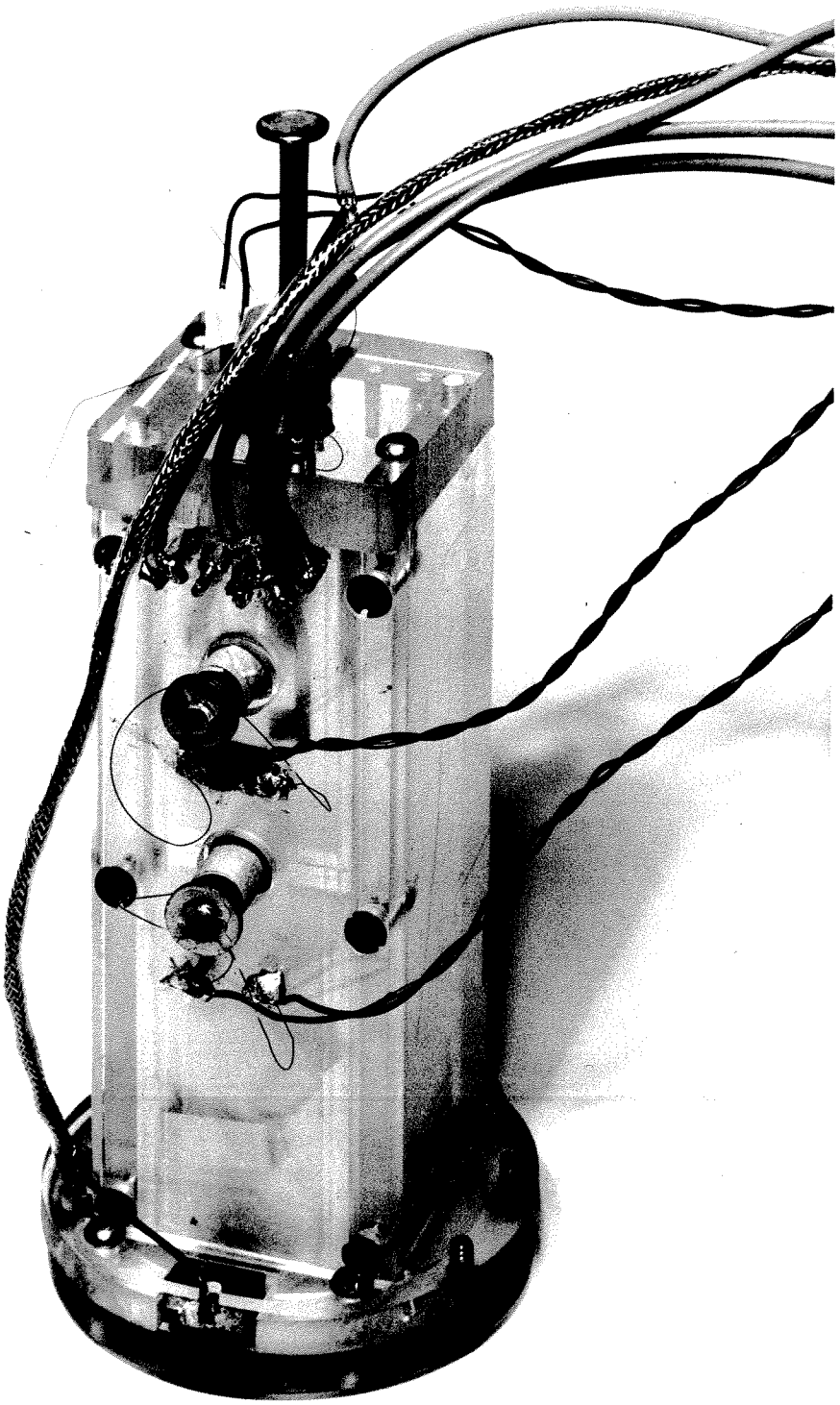

FIGURE I SECOND SOUND SHOCK TUBE WITH HEATER, SIDEWALL DETECTORS, AND CENTER PROBE INSTALLED

FIGURE 2 TYPICAL NICHROME HEATER WITH COPPER LEADS

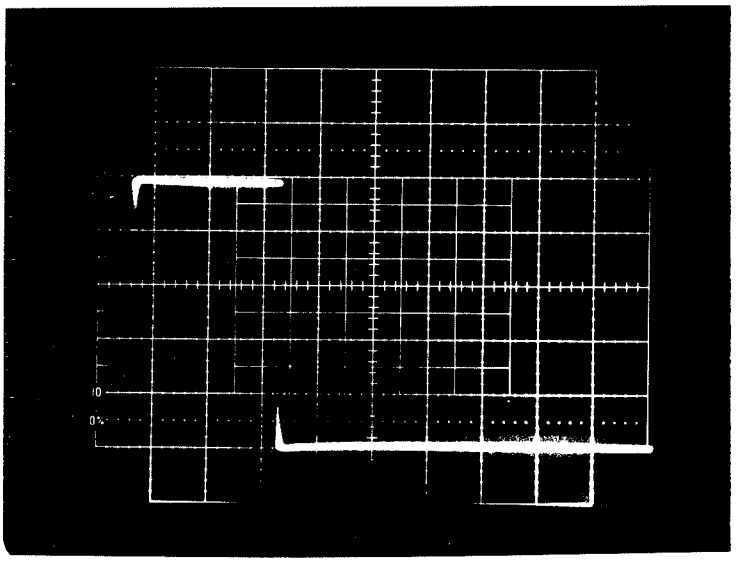

5 volt/div
0.5 m sec/div

FIGURE 3 OSCILLOSCOPE TRACE OF TYPICAL HEATER VOLTAGE PULSE

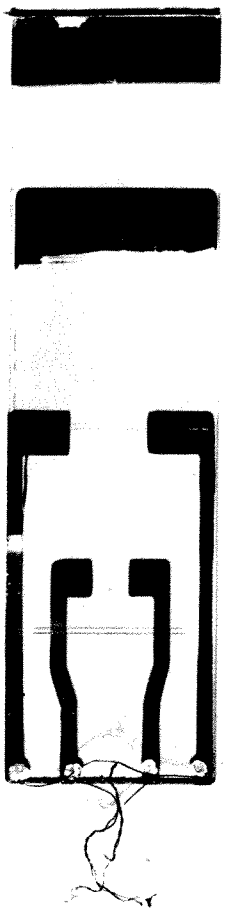

FIGURE 4 TYPICAL GOLD ON TIN SIDEWALL DETECTOR SLIDE

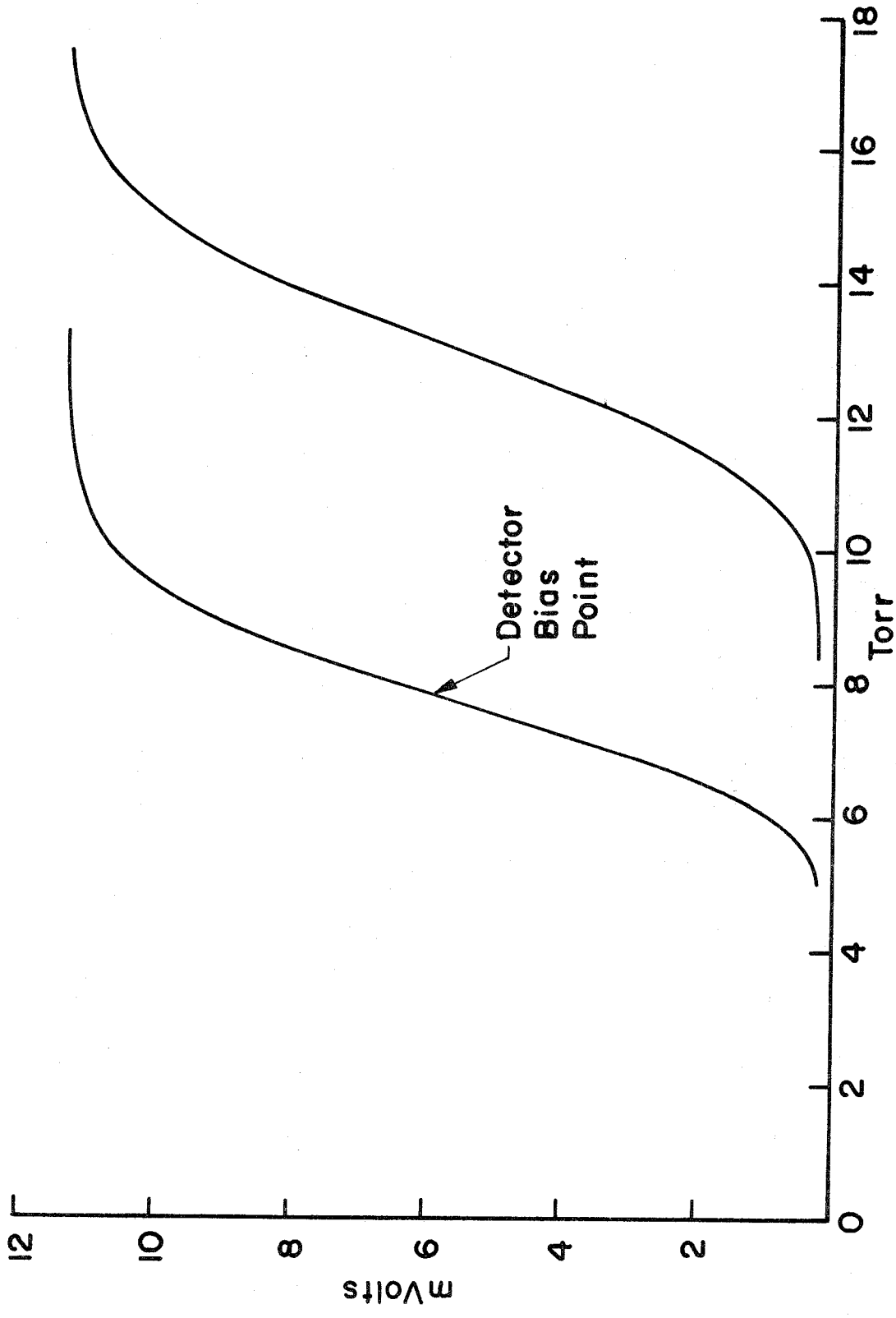

FIGURE 5 TYPICAL DETECTOR VOLTAGE BIAS CURVES FOR VARIOUS APPLIED MAGNETIC FIELDS

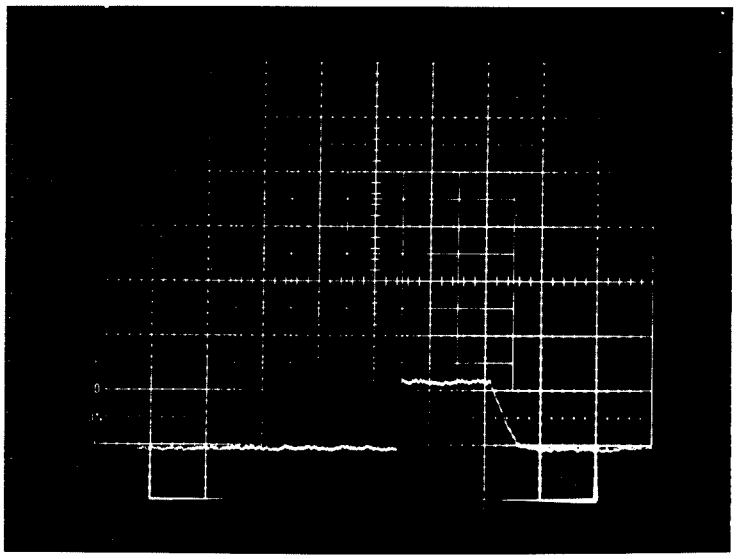

$T_o = 1.64\,^{\circ}K$

2.35 mK/div

50 μ sec/div

FIGURE 6 TYPICAL OSCILLOSCOPE TRACE OF SECOND SOUND SHOCK WAVE AS MEASURED BY A SUPERCONDUCTING DETECTOR

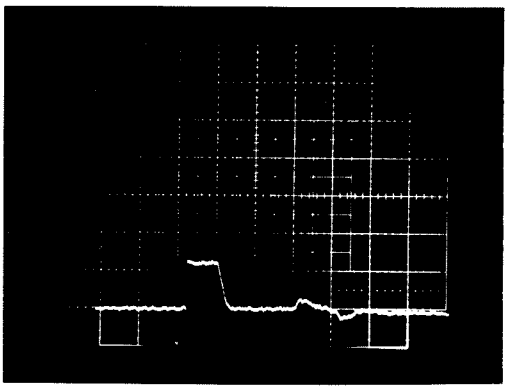

7a. 2.35 mK/div
100 μ sec/div

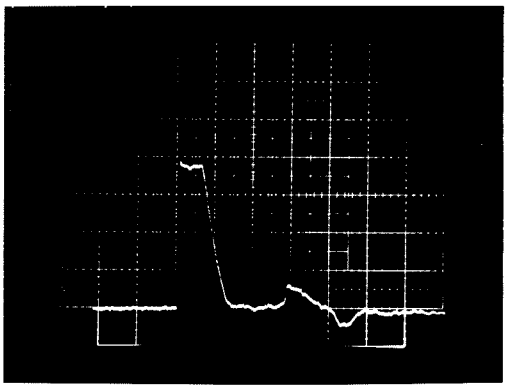

7b. 2.35 mK/div
100 μ sec/div

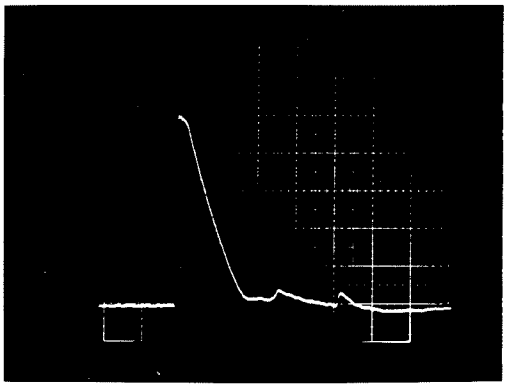

7c. 4.70 mK/div
100 μ sec/div

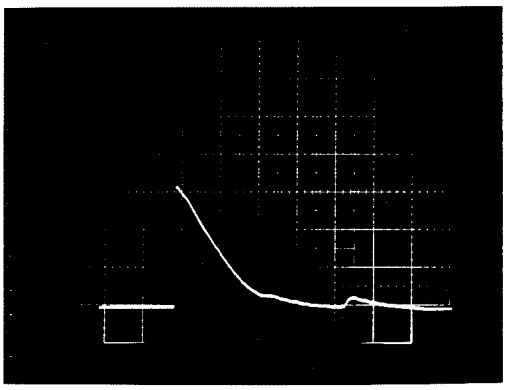

7d. 9.45 mK/div
100 μ sec/div

$T_o = 1.64\,^\circ K$

FIGURE 7 TYPICAL VARIATION OF HEAT PULSE SHAPE AS TRAILING EDGE OVERTAKES SECOND SOUND SHOCK

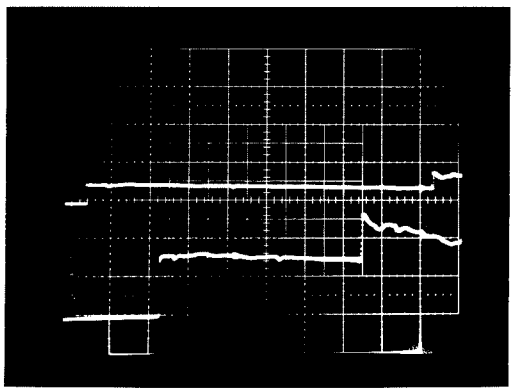

8a. upper trace: 5 m volt/div
lower trace: 500 m volt/div
horizontal: 500 μ sec/div
10 m sec Heat Pulse
T_o = 1.68 °K

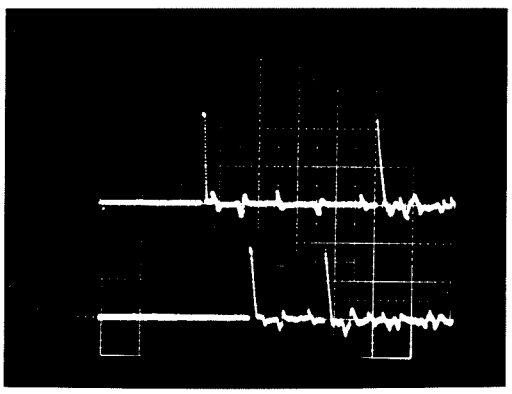

8b. upper trace: 100 m volt/div
lower trace: 500 m volt/div
horizontal: 1.0 m sec/div
100 μ sec Heat Pulse
T_o = 1.63 °K

FIGURE 8 OSCILLOSCOPE TRACES SHOWING SECOND SOUND SHOCK WAVE REFLECTION FROM AN ENDWALL

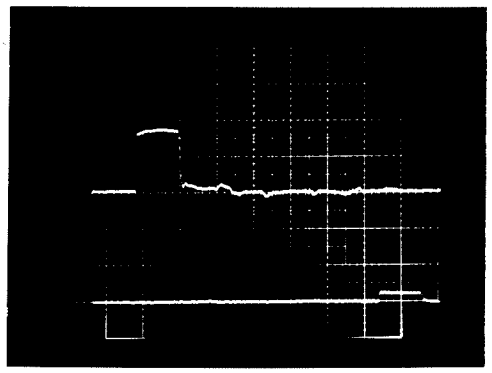

250 μ sec pulse duration
1.35 mK/div
200 μ sec/div

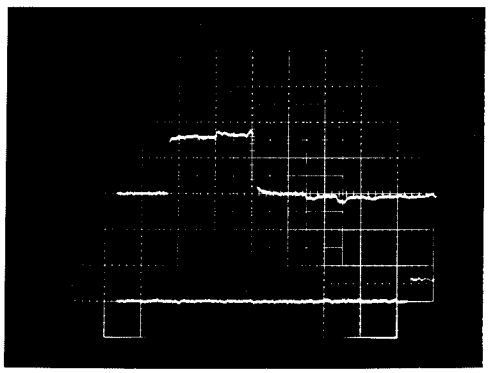

500 μ sec pulse duration
1.35 mK/div
200 μ sec/div

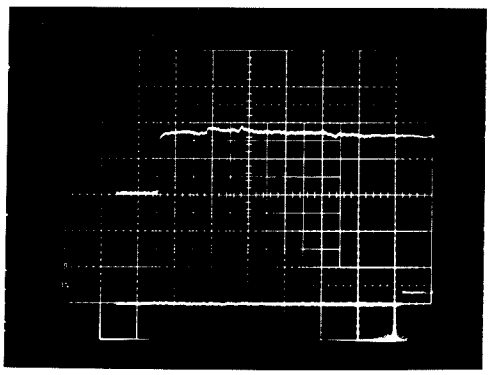

10 m sec pulse duration
1.35 mK/div
200 μ sec/div

FIGURE 9 OSCILLOSCOPE TRACES OF TYPICAL HEAT PULSES GENERATED BY VARIOUS DURATION VOLTAGE PULSES, T_o = 1.64°K

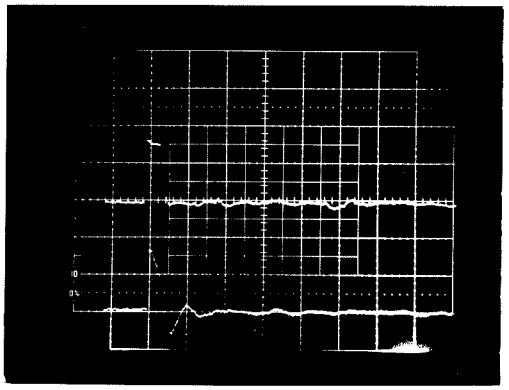

10a. 100 μ sec pulse

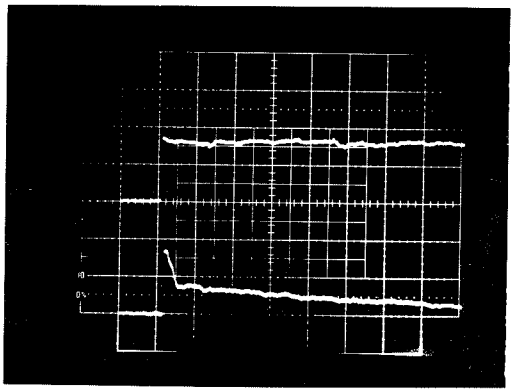

10b. 10 msec pulse

upper trace: 3.34 mK/div, sidewall detector
lower trace: 5.09 mK/div, center probe detector
horizontal: 200 μ sec/div

T_o = 1.63 °K

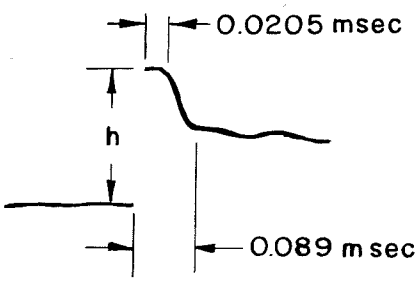

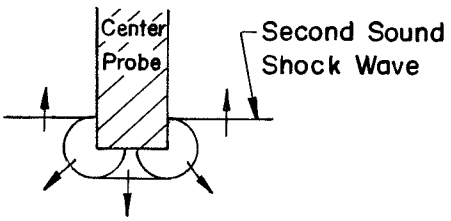

10 c.

FIGURE 10 SECOND SOUND SHOCK WAVES AS MEASURED BY SIDEWALL DETECTOR AND CENTER PROBE

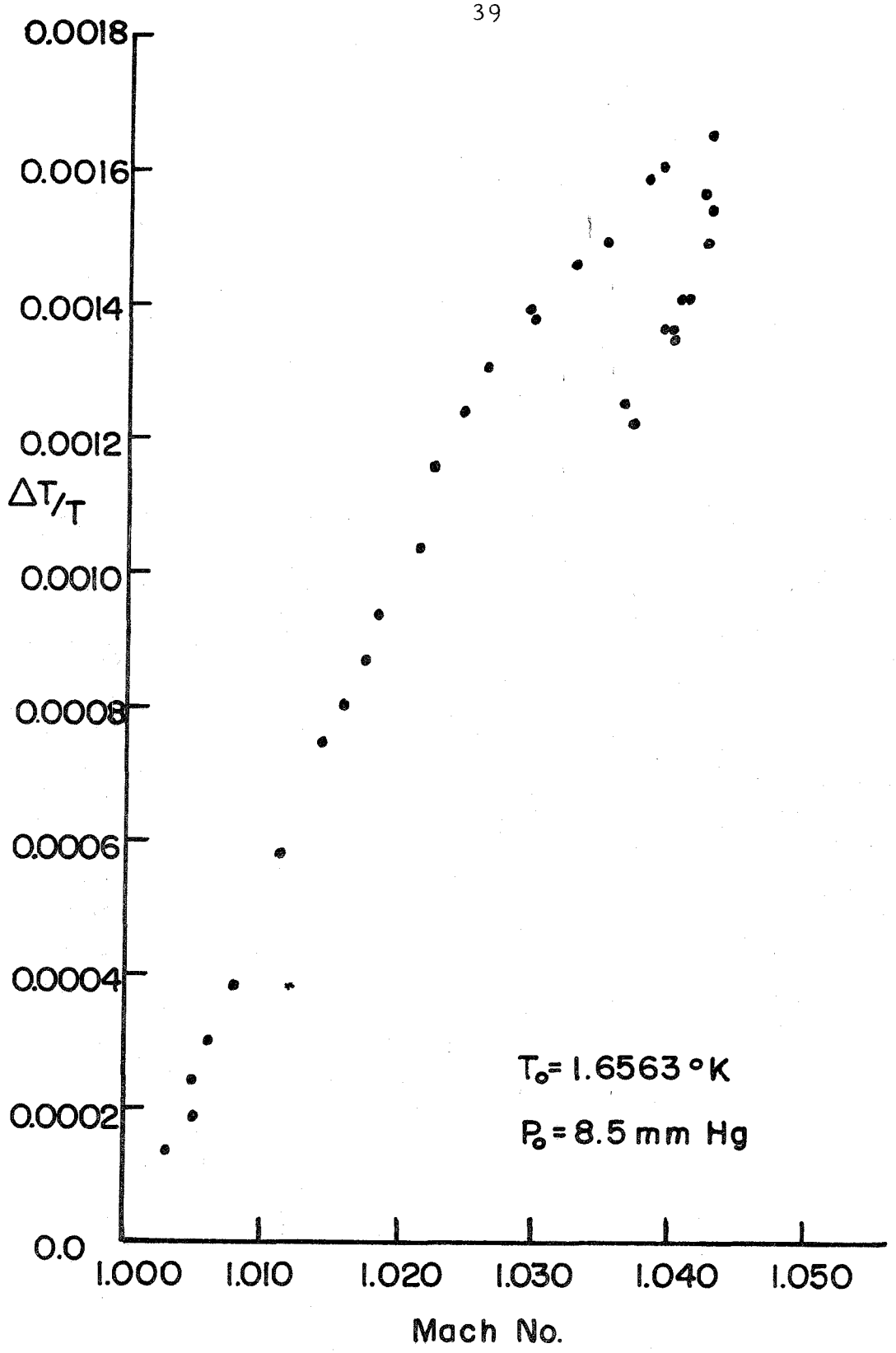

FIGURE 11 PLOT OF SHOCK STRENGTH VS. M, TANTALUM DETECTOR

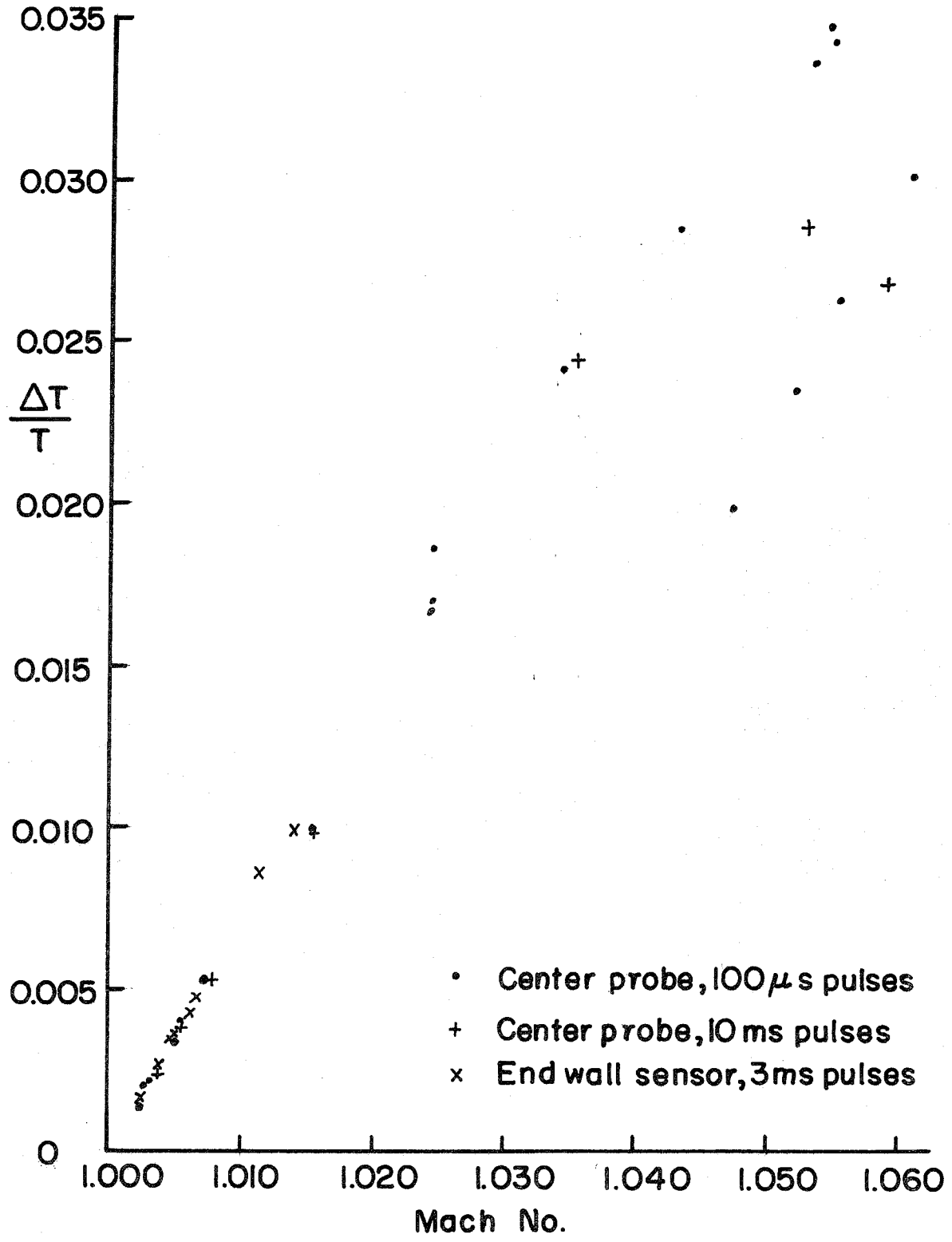

FIGURE 12 PLOT OF SHOCK STRENGTH VS. M, TIN ON GOLD ENDWALL DETECTOR AND CENTER PROBE

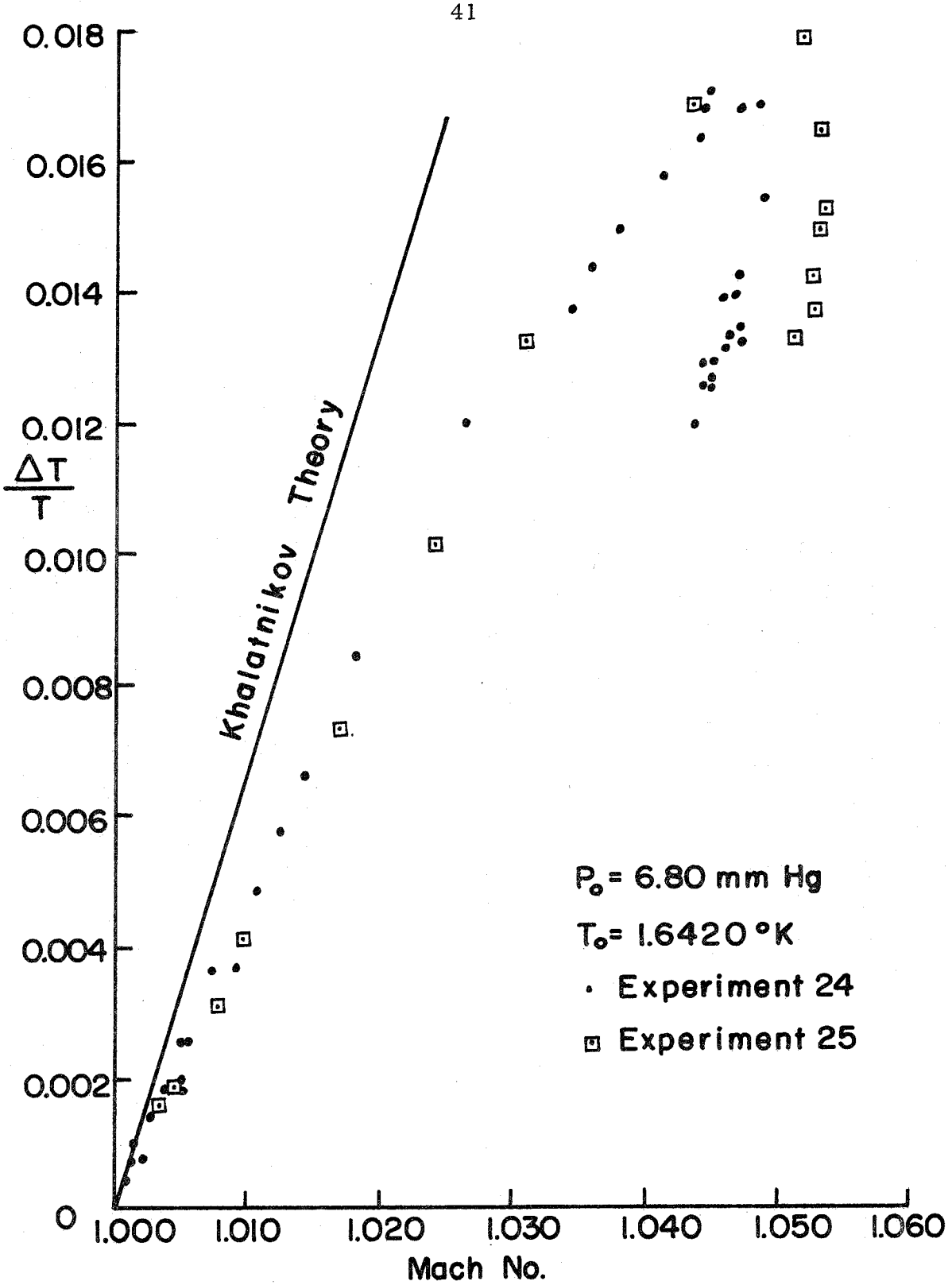

FIGURE 13 PLOT OF SHOCK STRENGTH VS M, TIN ON GOLD SIDEWALL DETECTORS

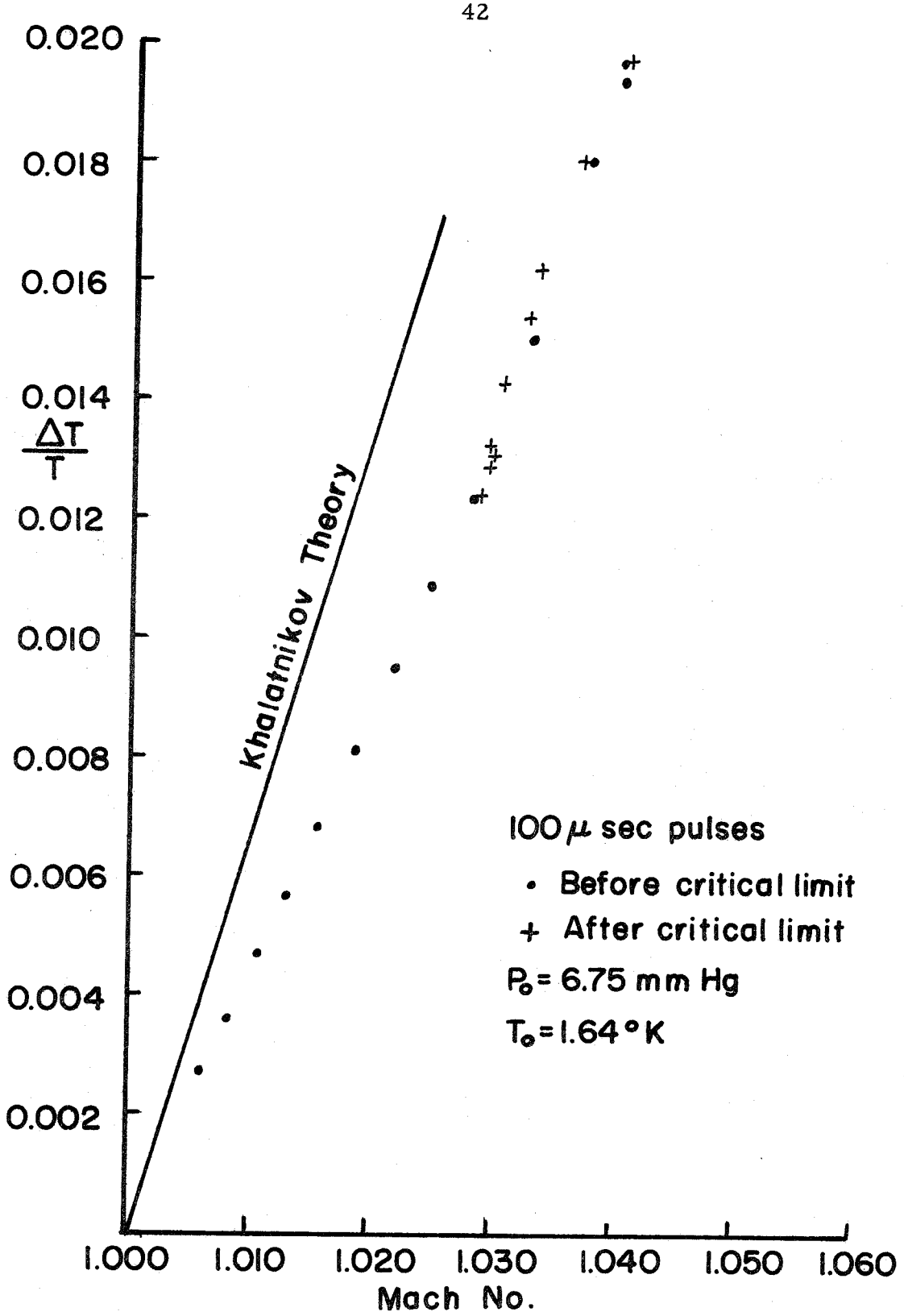

FIGURE 14 PLOT OF SHOCK STRENGTH VS. M, GOLD ON TIN DETECTOR TO DETECTOR

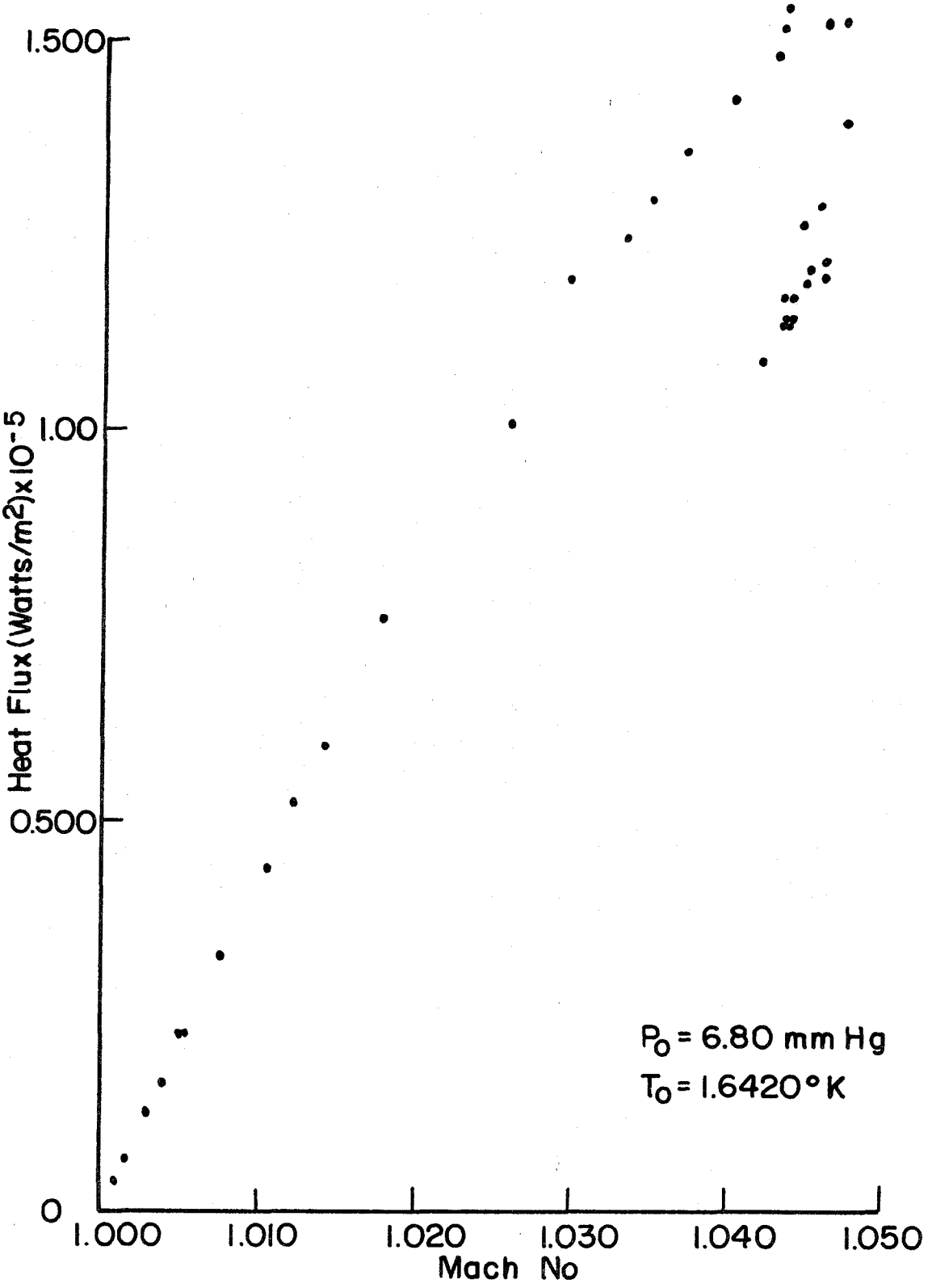

FIGURE 15 PLOT OF HEAT FLUX VS. M, EMITTER TO DETECTOR MEASUREMENTS

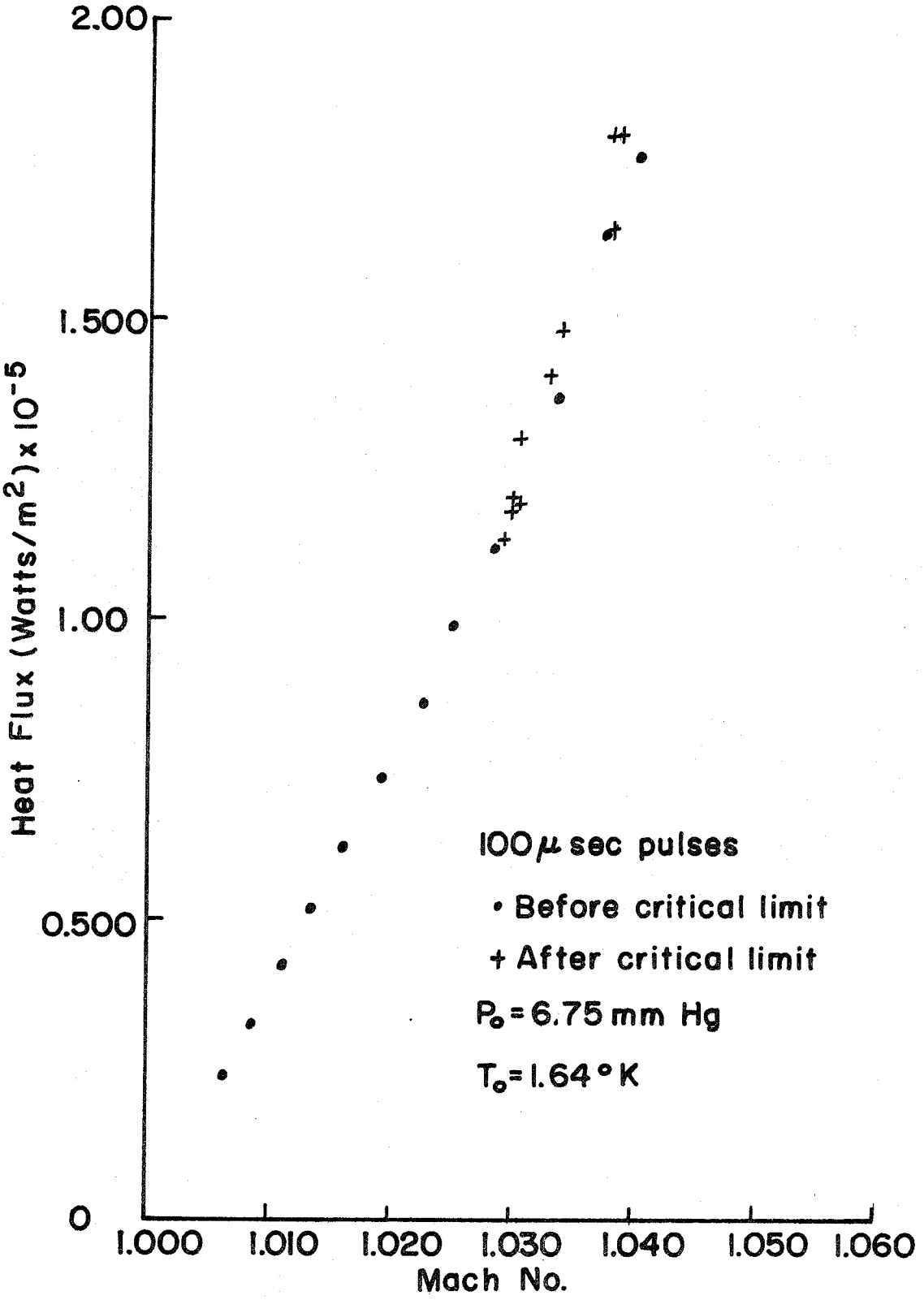

FIGURE 16 PLOT OF HEAT FLUX VS. M, DETECTOR TO DETECTOR MEASUREMENTS

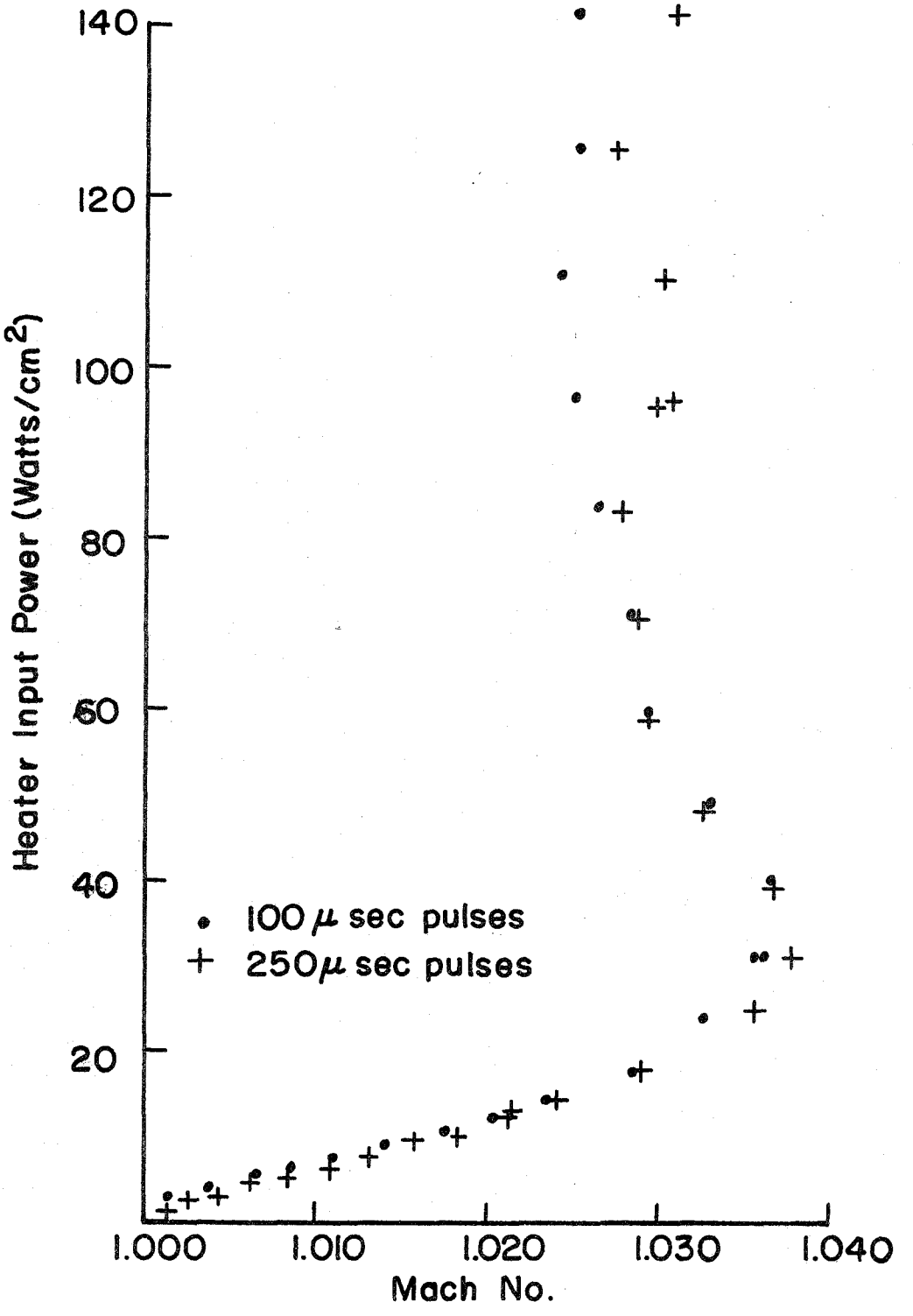

FIGURE 17 HEATER INPUT POWER VS. M, SIDEWALL DETECTOR

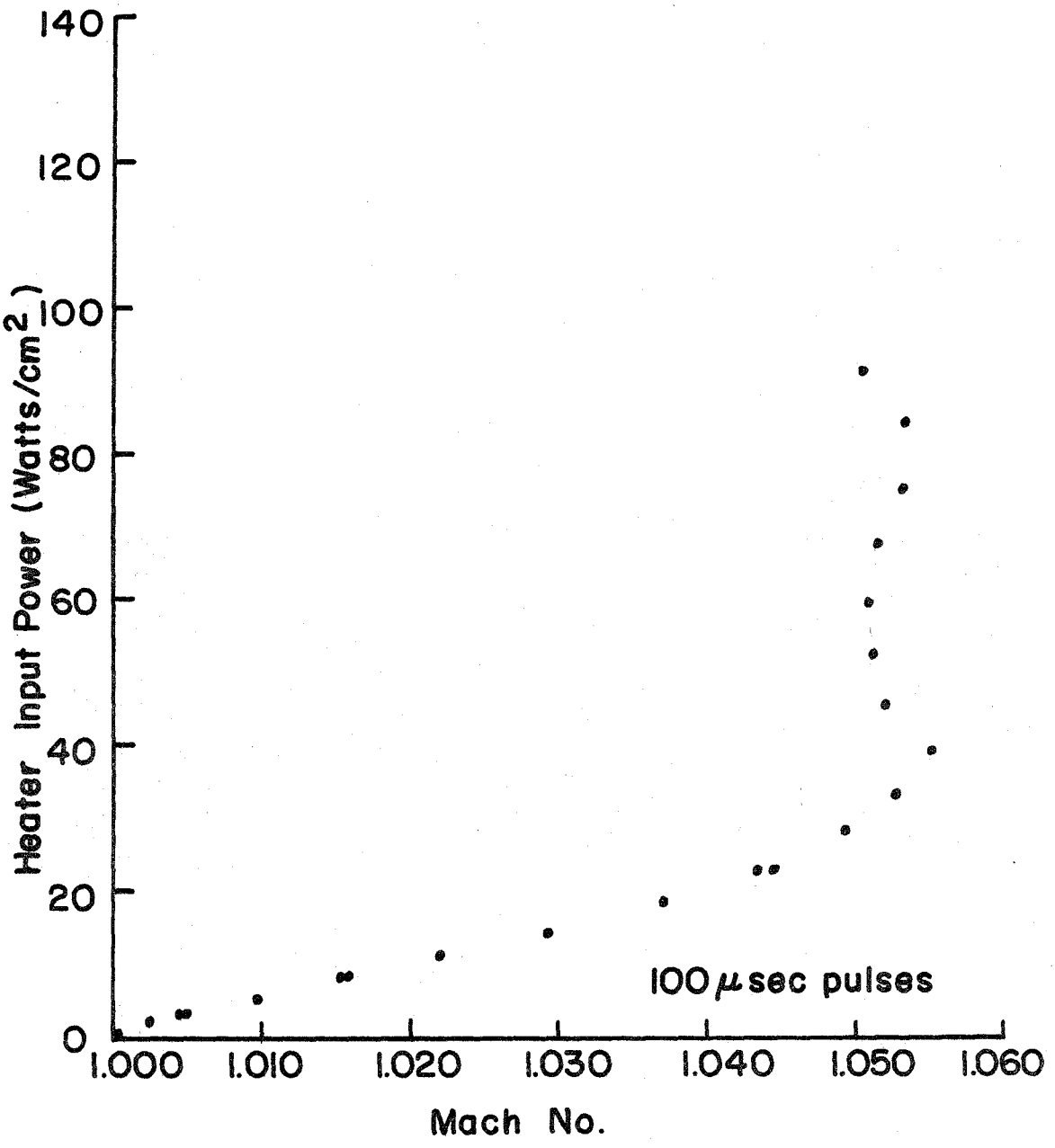

FIGURE 18 HEATER INPUT POWER VS. M, CENTER PROBE DETECTOR